

# Polymeric microellipsoids with programmed magnetic anisotropy for controlled rotation using low ( $\approx 10$ mT) magnetic fields

Andrea Bonilla Brunner<sup>1</sup>, Isabel Llorente García<sup>2</sup>, Bumjin Jang<sup>3</sup>, Midori Amano Patiño<sup>4</sup>, Viraj Alimchandani<sup>1</sup> Bradley J. Nelson<sup>3</sup>, Salvador Pané<sup>3</sup> and Sonia Contera<sup>1\*</sup>

<sup>1</sup> Clarendon Laboratory, Department of Physics, University of Oxford, Parks Road, OX1 3PU, UK

<sup>2</sup> Department of Physics and Astronomy, University College London, Gower Street, London, WC1E 6BT

<sup>3</sup> Multi-Scale Robotics Lab (MSRL), Institute Swiss Federal Institute of Technology (ETH) Zurich, Tannenstrasse 3 CH-8092, CLA H9

<sup>4</sup> Institute for Chemical Research, Kyoto University, Uji, Kyoto 611-0011, Japan

\*Corresponding author: Sonia.AntoranzContera@physics.ox.ac.uk

## Abstract

Polymeric magnetic spherical microparticles are employed as sensors/actuators in lab-on-a-chip applications, small-scale robotics and biomedical/biophysical assays. Achieving controlled stable motion of the microparticles in a fluid environment using low intensity magnetic fields is necessary to achieve much of their technological potential; this requires that the microparticle is magnetically anisotropic, which is difficult to achieve in spheres. Here we have developed a simple method to synthesise anisotropic ellipsoidal microparticles (average eccentricity  $0.60 \pm 0.14$ ) by applying a magnetic field during synthesis, using a nanocomposite of polycaprolactone (PCL) with  $\text{Fe}_3\text{O}_4$  nanowires. The “microellipsoids” are thoroughly characterised using optical microscopy, scanning electron microscopy (SEM), transmission electron microscopy (TEM) and energy dispersive X-ray spectroscopy (EDX). Their suitability for magnetically controlled motion is demonstrated by analysing their rotation in low magnetic fields (0.1, 1, 5, 10 and 20 mT) at varying rotational frequencies (1Hz and 5Hz). The microellipsoids are able to follow smoothly and continuously the magnetic field, while commercial spherical particles fail to continuously follow

31 the magnetic field, and oscillate backwards and forwards resulting in much lower average angular  
32 speeds. Furthermore, only 23% of commercial particles analysed rotated at 1 Hz and 26% at 5 Hz,  
33 whereas 77% of our ellipsoidal particles rotated at 1 Hz, and 74% did at 5 Hz.

34

## 35 **Keywords**

36 Magnetic microparticles, polymeric microparticles, micromanipulation, programmed magnetic  
37 anisotropy, microfluidics, microrobots

38

## 39 **1. Introduction**

40 Magnetic polymer composites (MPCs) are widely used in microsystems and microrobotics as they  
41 simultaneously feature the processability and facile chemical functionalisation of polymers, and the  
42 possibility of using magnetic fields for actuation by exploiting the magnetic properties of the  
43 embedded nanostructures.[\[1-3\]](#) Magnetic fields are often preferred as external force generators due  
44 to their non-invasiveness, biological inertness, and better performance in comparison to other  
45 methods such as acoustic waves (including ultrasound) and electric fields.[\[4\]](#)

46 MPC-based microstructures can be used to perform tasks in handling and assembling small objects  
47 and biological molecules, or sensing physical, biological or chemical molecules or functions.[\[1, 5-7\]](#) In  
48 particular, MPCs shaped into spherical beads have been preferred as a favourite architecture for  
49 small-scale mechanical technologies due to the ease of fabrication, versatility and suitability for  
50 theoretical modelling. Spherical magnetic beads already play an important role in microfluidics; they  
51 can be made to link to target species and can be used for manipulation and/or detection in lab-on-a-  
52 chip systems[\[8-10\]](#) and protein and biomolecular purification and mixing. They are also used for  
53 generating and measuring forces at the micrometre scale in biophysical studies,[\[11-13\]](#) in torque-  
54 generating assays,[\[14\]](#) cellular mechanotransduction and microrheology, in magnetic twisting  
55 cytometry,[\[15, 16\]](#) in cellular, protein and nucleic acid manipulation in separation assays,[\[17\]](#) in  
56 immunoassays,[\[18\]](#) in magnetic flow cytometry,[\[19\]](#) in magnetic separation in lab-on-a-chip  
57 microfluidic systems,[\[20\]](#) in directed hyperthermia applications[\[11, 21\]](#) and targeted drug  
58 delivery.[\[22\]](#) Most applications use commercial spherical MPC microparticles consisting of a  
59 polymeric matrix that confines magnetic spherical superparamagnetic Fe<sub>3</sub>O<sub>4</sub> nanoparticles (NPs).

60 The particular case of anisotropic microparticles has attracted a significant attention over the past  
61 two decades [\[23\]](#). Particle anisotropy can be conveyed by fabricating non-spherical shapes and/or  
62 non-uniform surface properties. In both cases, their physical properties differ from those of isotropic

63 microparticles, making them potentially useful for assembly e.g. colloidal substitutes for liquid  
64 crystals and electrorheological fluids [24] [25], designing photonic crystals with novel symmetries,  
65 controlling suspensions' rheology [26] and suspensions' optical properties [27], stabilizing emulsions  
66 [28] and stabilizing foams [29], engineering of biomaterials [30] and colloidal composites [31].

67 Beyond building structure, anisotropic particles are also useful for engineering dynamics at the  
68 microscale and actuation. In order to perform complex tasks and movements such as controlled  
69 rotation it is necessary to exert torque on the particle. One way of exerting magnetic torque on  
70 materials exhibiting magnetic moment is by controlling their shape anisotropy, which e.g. gives way  
71 to an easy-axis of magnetisation along the longest dimension in disks and rods. In a magnetic field,  
72 the most energetically favourable configuration is achieved when the easy axis of magnetisation  
73 aligns parallel to the direction of the applied field, producing rotation towards it [4, 32].

74 One of the main drawbacks of using spherical microparticles confining NPs is that they have  
75 relatively low shape anisotropy (as we demonstrate later in the results section), and require high  
76 magnetic fields to align all of the magnetic moments of the NPs inside of them [21]. To obtain a  
77 more controlled magnetic response several strategies aimed at programming magnetic anisotropy in  
78 the structure have been developed [2, 33]. Often these have involved top-down approaches such as  
79 inkjet printing [2] or photopatterning [33]. The applications of magnetic anisotropic particles  
80 include: (i) Fluid mixing in microfluidics and biosensing in small volumes of liquid: sample flow in  
81 small volumes and miniaturized channels is laminar [34]; and turbulent mixing between two liquids  
82 cannot be achieved. In lab-on-a-chip and microfluidic devices, it is crucial to attain a fast and  
83 adjustable mixing in applications in which several reactants or specimens are used. A magnetic  
84 microparticle that is able to rotate can be deployed in almost any environment to produce  
85 turbulence. This can find practical applications beyond mixing of reagents, for example, in extraction  
86 of specific micro/nano objects from a solution as they can be functionalized with specific molecules,  
87 proteins, bacteria or viruses. Turbulent flow can aid adsorption, prevents clustering of the target  
88 molecules/cells/microorganisms and from adhering to the container walls [35]. And (ii) biophysical  
89 assays: optical tweezers based on trapping polymer-based microbeads has revolutionized our  
90 understanding in motion in biological systems such as molecular motors, including the actions of  
91 ATP-synthases and bacterial flagellar motors. However, optical tweezers present drawbacks such as  
92 overheating of the samples. Magnetic tweezers are a promising alternative. However, they are  
93 currently used to manipulate commercial spherical microparticles, which prevents the advancement  
94 of the field, due to their intrinsic variability of their rotational behavior [14, 36].

95 Here we have synthesised magnetic nanocomposite microellipsoids based on a matrix of  
96 polycaprolactone (PCL) by a simple oil-in-water emulsion method. The polymer microellipsoids are

97 formed in the emulsion in the presence of magnetite nanowires ( $\text{Fe}_3\text{O}_4$ ), which are trapped in the  
98 particle matrix. During the synthesis, DC magnetic fields are used to align the nanowires and create  
99 magnetic (shape) anisotropy. The particles are thoroughly characterised using optical microscopy,  
100 scanning electron microscopy (SEM), transmission electron microscopy (TEM) and energy dispersive  
101 X-ray spectroscopy (EDX). Furthermore, the superior rotation properties at low magnetic field  
102 intensity in comparison to commercially available microparticles is demonstrated using rotating  
103 magnetic fields with field strengths of 0.1, 1, 5, 10 and 20 mT, at varying rotation frequencies (1Hz  
104 and 5Hz).

105

## 106 2. Materials and Methods

### 107 2.1 Nanowire synthesis

108  $\text{Fe}_3\text{O}_4$  nanowires were prepared by hydrolysis of  $\text{Fe}^{3+}$  [37]. Briefly, a solution consisting of 420 mM  
109  $\text{FeCl}_3 \cdot 4\text{H}_2\text{O}$ , 210mM  $\text{FeSO}_4 \cdot 7\text{H}_2\text{O}$  and 1M  $(\text{NH}_2)_2\text{CO}$  (all chemicals from Sigma Aldrich, UK) was  
110 prepared with deoxygenated Milli-Q water (Nitrogen flow for 30 minutes) and stirred for 10 minutes.  
111 The solution was then added to a Teflon flask and placed in an autoclave reactor. A 0.45T NdFeB  
112 magnet (First4magnets, UK) was positioned in the bottom of the autoclave to induce nanowire  
113 growth on the easy axis [38]. The reactor was placed in an oven at 130°C for 6 hours. After this time,  
114 the reactor was allowed to cool down at room temperature overnight. The resulting black magnetic  
115 dispersion was washed 3 times with deoxygenated water and freeze dried for 24 hours.

116

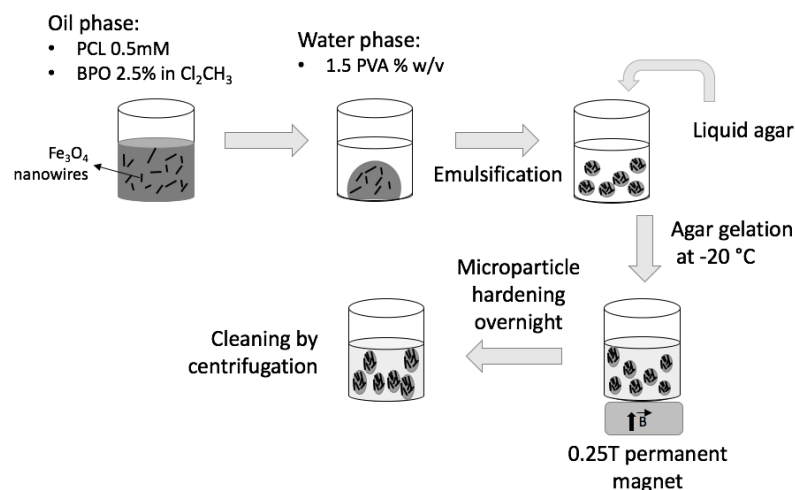
### 117 2.2 Microellipsoid synthesis

118 Microellipsoids were synthesised by using the oil-in-water emulsion method, as illustrated in Fig. 1.  
119 The oil phase contained luperox (benzoyl peroxide, Sigma Aldrich) (2.5% w/v), which acted as the  
120 initiator of PCL crosslinking, dissolved in dichloromethane at 0.5 mM. Synthesised  $\text{Fe}_3\text{O}_4$  nanowires  
121 (described above) were dispersed in the PCL solution at a concentration of 0.5% (w/v) which is at  
122 least 20 times smaller concentration than commercial particles ( $\approx 10$  to 39% of  $\text{Fe}_3\text{O}_4$  content  
123 depending on the manufacturer). In order to achieve a homogeneous dispersion of nanowires in the  
124 oil phase, the solution was sonicated in a water bath for 5 minutes.

125 The water phase consisted of soluble poly(vinyl alcohol) (PVA, Sigma Aldrich, UK) (1.5% w/v)  
126 as a non-surfactant stabilizer. The oil phase was emulsified by adding it dropwise into the water  
127 phase while stirring at 3,000 rpm (MS1 Minishaker IKA, UK), and emulsified for 10 minutes at this

128 speed. Liquid agar (1% w/v) was immediately added, mixed for 3 minutes and settled in the freezer  
 129 at -20°C for 10 minutes. Liquid agar was used to immobilize the microellipsoids, preventing them to  
 130 collect back together into a bigger oil phase droplet, hence allowing them to harden individually. A  
 131 static magnetic field of 0.25 T was applied during hardening to modify the orientation of the  
 132 nanowires embedded within the polymeric structure. The gel was aged at room temperature  
 133 overnight to allow particle hardening. Finally, microellipsoids were cleaned and sorted by size using  
 134 density gradient centrifugation with a glucose column, at 3,000 rpm for 7 minutes. The smallest  
 135 microellipsoid (those corresponding to the first layer of the gradient) were used for this study. The  
 136 microellipsoids were rinsed 3 times with ultrapure deionized (DI) water (Millipore MilliQ, UK) and  
 137 kept at 4°C. The dimensions distribution of the ellipsoid are given in the Fig. 2S in the supplement.

138



139

140 Figure 1. Schematic representation of the oil-in-water emulsion synthesis of the microellipsoids. The oil  
 141 phase contains benzoyl peroxide (2.5% w/v) and 0.5 mM PCL dissolved in dichloromethane with 0.5%  
 142  $\text{Fe}_3\text{O}_4$  nanowires dispersed. The water phase consists of PVA 1.5% w/v. The oil phase was emulsified into  
 143 the water phase by stirring. Liquid agar (1% w/v) was immediately added and settled at -20 °C during  
 144 microellipsoid hardening in the presence of a static magnetic field of 0.25 T. Particles were left at room  
 145 temperature overnight to allow PCL hardening while inducing orientation of the nanowires and creating  
 146 the ellipsoidal shape.

147

### 148 2.3 Microellipsoid characterisation. TEM and SEM imaging

149 The microstructure and phase of the nanowires and the microellipsoids were analysed by TEM on a  
 150 FEI Talos F200X instrument operated at 200 keV acceleration voltage. Both, TEM and scanning TEM  
 151 (STEM) operation modes of the instrument were used for the study. STEM studies were performed  
 152 in the high angle annular dark field (HAADF STEM) imaging mode and accompanied by elemental

153 content analysis using energy dispersive spectroscopy EDX STEM. STEM and EDX STEM studies were  
154 carried out using a 0.8 nm probe size.

155 SEM images were acquired by a secondary electron detector in a Zeiss ULTRA 55 apparatus.  
156 The sample was dispersed on a Si wafer and dried.

157

## 158 **2.4 Rotation experiments**

159 The rotational motion of microellipsoids was characterised using a commercial magnetic actuation  
160 system (MFG-100-i, Magnebotix, Switzerland) mounted on an optical microscope (Olympus IX,  
161 Olympus). The magnetic actuation system consists of 4 pairs of solenoid coils which allow 3D  
162 manipulation of micrometer-size magnetic objects. Experiments were carried out in ultrapure DI  
163 water deionized water (Millipore MilliQ) applying various magnetic field amplitudes (0.1, 1, 5, 10 and  
164 20 mT) for fields rotating at two different frequencies (1 and 5 Hz). Commercial superparamagnetic  
165 spherical polystyrene beads (nominal diameter: 2.0-2.9  $\mu\text{m}$ , SPHERO™ Magnetic Particles: PM-20)  
166 were assessed as a control. Particle motion was recorded using a CCD camera (SCA 1400, Basler) at  
167 30 frames per second (fps).

168

## 169 **2.5 Image processing to analyse the rotation of the microellipsoids.**

170 A suite of image processing algorithms for single particle rotational tracking was custom-written in  
171 Matlab to quantitatively extract the orientation of all particles in each acquired video sequence. The  
172 program automatically detects all microellipsoids in each video frame via intensity thresholding. This  
173 operation results in a binary image with connected regions, i.e., masks, for each particle on top of a  
174 zero background. The ellipse that best fits the shape of each particle mask shape is then found to  
175 extract the particle centre-of-mass, major and minor axis lengths and orientation angle of the major  
176 axis with respect to the horizontal image axis. The eccentricity is calculated for each microellipsoid  
177 using the obtained major and minor axis lengths. Single-particle tracking is then achieved by linking  
178 particles found on subsequent frames. The linking decision is based on comparing the pair-wise  
179 distances between each particle on a given frame and all particles on the previous frame and  
180 choosing the assignment with the smallest pair-wise distance. After all tracking assignments are  
181 made, the result is a set of particle trajectories for each video analysed, so that the orientation angle  
182 of the particles as a function of time can be analysed.

183 The angular velocity of all the rotating colloids during uniform rotation (excluding  
184 oscillations) was calculated for particles that completed at least one 360° turn. Additionally, the  
185 effective frequency of rotation (number of full turns per second) of the colloids subjected to small  
186 field intensities (0.1 and 1 mT) was also quantified.

187

### 188 3. Results and discussion

#### 189 3.1 Structural characterisation

190 Microellipsoids were synthesised as described in the materials and methods. The average  
191 microparticle yield is approximately 7 % for the particle size competent to this study (2-3 μm). This  
192 value is so low since the emulsification process lacks of particle size control, resulting in a high  
193 particle size dispersion.

194 Fig. 2 (a) shows two typical microellipsoids imaged by SEM displaying a clear ellipsoidal shape with  
195 different eccentricities ( $\epsilon$ ).  $\epsilon$  represents how ellipsoidal a particle is ( $\epsilon = 1$  for infinite rods and  $\epsilon = 0$   
196 for spheres), and is calculated using the formula:

$$197 \quad \epsilon = \sqrt{\frac{a^2 - b^2}{a^2}}, \quad 0 < \epsilon < 1, \quad [1]$$

198 for prolate ellipsoids with semiaxes a and b.

199 PCL microparticles fabricated without nanowires and in the absence of a magnetic field using  
200 this method present a spherical shape (Fig. A.1, supplementary material).

201 TEM was used to identify the arrangement of the Fe<sub>3</sub>O<sub>4</sub> nanowires within the particle (Fig. 2 (b)). The  
202 presence of a magnetic field during synthesis results in the formation of clusters (shown in Fig. 2 (c))  
203 which eventually determines the final ellipsoidal shape of the particle.

204 The images indicate that the magnetic field applied during the synthesis is not sufficient to align all  
205 the individual nanowires and overcome forces arising from the interaction between polymers and  
206 nanowires during crosslinking and colloid hardening. The formation of nanowire clusters could also  
207 be the result of attractive interactions between nanowires before the magnetic field was applied, or  
208 pre-clustering due to rotational forces during emulsification and particle formation from the oil  
209 phase. Despite this clustering, the magnetic field is sufficiently strong to orient clusters of wires so  
210 that the resulting particles exhibit an ellipsoidal shape. As a control, we performed the same  
211 synthesis protocol in the absence of a magnetic field (supplementary Materials A, Fig. A2); in this

212 case the most of the particles presented a spherical shape, highlighting the role of the magnetic field  
213 aligning the clusters during synthesis.

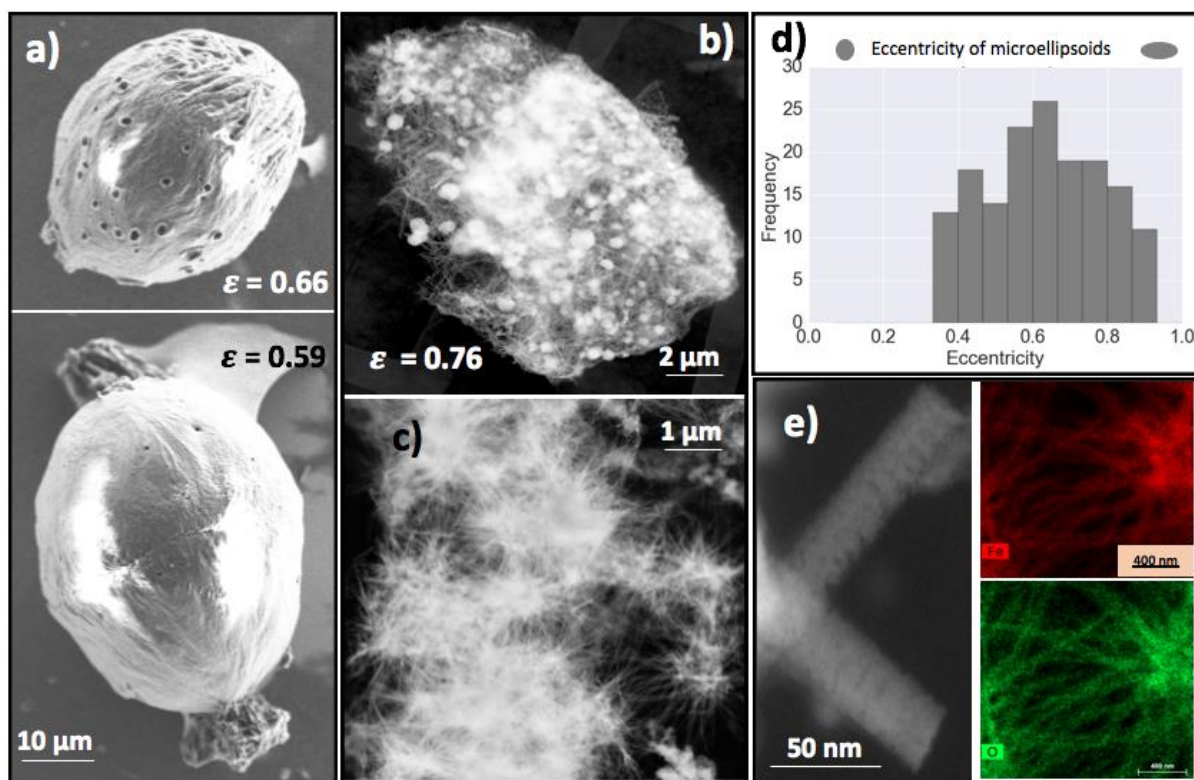
214 Future experiments regarding the fabrication of microparticles with nanoparticles embedded  
215 (instead of nanowires or nanoparticles attached to the surface) in the presence of an external  
216 magnetic field during hardening, could also, in principle, produce ellipsoidal shapes since  
217 nanoparticles could also align to the field producing stretching of the particle. *In general, the*  
218 *elongated shape of a magnetic composite in the presence of a magnetic field is energetically more*  
219 *favourable*. Previous work by Faraudo et al. [39] has shown that superparamagnetic microspheres  
220 can become aligned in certain conditions in fluid environments, where a key parameter is the  
221 magnetic coupling coefficient between the particles. However, due to their shape isotropy, a large  
222 magnetic gradient is needed for alignment even in water ( $10\text{--}30\text{ T m}^{-1}$ ). It is therefore reasonable to  
223 assume that producing alignment of nanoparticles in a polymeric matrix would require even larger  
224 magnetic fields that are not practical for a facile synthesis methods. Indeed, our results show that  
225 even with nanowires that are much larger and can align much easier than nanoparticles in a  
226 magnetic field, total alignment is not possible with the relatively low magnetic fields used in our  
227 work. However, the magnetic fields used in our paper succeed to produce ellipsoids by alignment of  
228 clusters of nanowires, which leads to the success of our initial purpose: to create anisotropic  
229 magnetic particles with a simple synthesis method.

230 In order to quantify  $\varepsilon$  for the microellipsoids,  $a$  and  $b$  were measured from optical microscopy  
231 images of the particles in solution as described above (Fig. B.1). The distribution of  $\varepsilon$  is shown in Fig.  
232 2 (d) for a total of 159 colloids analysed, confirming that the synthesis method clearly leads to  
233 ellipsoidal particles.

234 Finally, in Fig. 2 (e) we show a TEM analysis of individual nanowires. EDX analysis of the nanowires  
235 embedded within the polymeric PCL lattice is also shown in Fig. 2 (e), EDX allow us to identify that  
236 the nanowires consist of iron oxide, iron content is depicted in red and oxygen in green (see Fig. C.1  
237 for details).

238





239

240 Figure 2. a) SEM images of synthesised magnetic ellipsoidal particles with different eccentricities  $\epsilon$ . b)  
 241 TEM images of microellipsoids showing the nanowire structure embedded within the polymer matrix. c)  
 242 Nanowire cluster formation due to the presence of a magnetic field during microparticle hardening. d)  
 243 Histogram of  $\epsilon$  values of the microellipsoids. e) TEM image of synthesised  $\text{Fe}_3\text{O}_4$  nanowires and EDX  
 244 analysis showing the structural composition of the nanowires (supplementary data, Fig. S3).

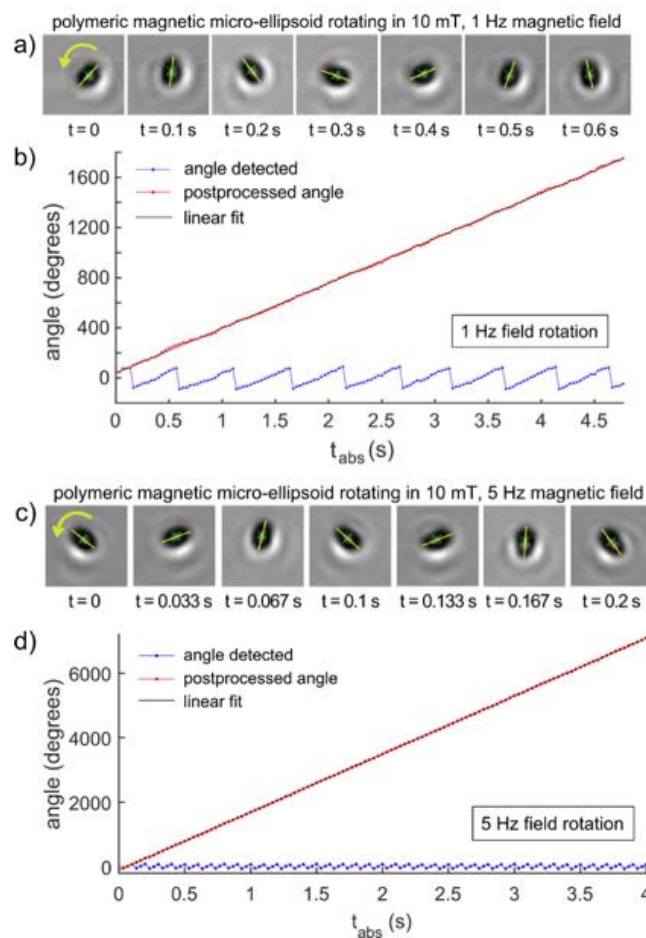
245

### 246 3.2 Angular velocity of the ellipsoidal colloids and comparison with commercial 247 spherical colloids

248 In order to evaluate the performance of the microparticles, we monitored and analysed their  
 249 movement subject to rotating magnetic fields, using the automatic method described in the  
 250 materials section. Two examples of the application of the method are given in Fig. 3. Fig. 3 (a)  
 251 displays a typical time sequence for the rotation of one of the microellipsoids in the presence of a 10  
 252 mT magnetic field rotating at a frequency of 1 Hz. Fig. 3 (c) shows a sequence for a different particle  
 253 and a 10 mT magnetic field rotating at 5 Hz. The initial orientation angle detected is between -90  
 254 degrees and +90 degrees, and smooth particle rotation with constant angular velocity is indicated by  
 255 the clear periodicity and linearity of the angle versus time (blue traces in Figs. 3 (b) and 3 (d)).

256 Further processing of the angle is carried out by automatically detecting orientation jumps in the  
 257 data and assuming anti-clockwise rotation to generate a monotonically increasing positive angle (red

258 traces in Figs. 3 (b) and 3 (d)). This can be fitted to a line (solid black lines in Figs. 3 (b) and 3 (d)) to  
 259 obtain from the slope the angular velocity and frequency of rotation of the microparticle. For  
 260 particles that display uneven rotation with non-constant angular velocity, jumps or angle oscillations,  
 261 only linear segments (detected automatically in the angle-versus-time data) of approximately  
 262 constant angular velocity are fitted to a line. An average rotation frequency is then calculated as the  
 263 mean of the frequencies corresponding to all rotation segments in these cases. Particle trajectories  
 264 with less than 10 frames and rotation segments with less than 5 frames are excluded from the  
 265 analysis. Only isolated particles are analysed (particles that clump together into large clusters are  
 266 discarded for the analysis).



267

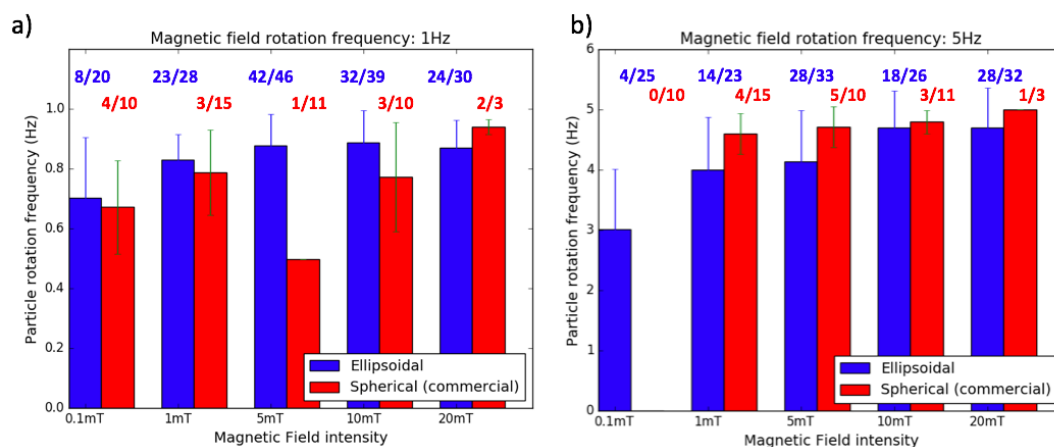
268 Figure 3. Quantitative extraction of particle rotation angle and frequency via image processing. a)  
 269 Sequence of image frames acquired for one of our polymeric magnetic microellipsoids rotating in a 10  
 270 mT, 1 Hz rotating magnetic field. Every third frame acquired is shown. Yellow lines indicate the angle  
 271 found for the particle. Green crosses indicate the found centre-of-mass. The rotation of the field and  
 272 particle is counter-clockwise as indicated by the rotation arrow on the first frame. b) Orientation angle  
 273 versus time for a  $\sim 5$ -second-long rotation sequence corresponding to the particle shown in a). The fit of  
 274 the post-processed angle (see text) yields a particle rotation frequency of  $(0.996 \pm 0.001)$  Hz, very close to  
 275 the field-rotation frequency. c) Rotation time sequence for one of our particles in the presence of a 10  
 276 mT, 5 Hz rotating magnetic field. Every frame acquired is shown. d) Orientation versus time for the

277 particle rotating in the 5 Hz field. The linear fit yields a particle rotation frequency of  $(4.995 \pm 0.001)$  Hz.  
278 Note that the depicted particle presents a selected case where smooth rotation following the rotation of  
279 the magnetic field is achieved, yet some particles deviate from this ideal performance. Figure. 4 shows the  
280 dispersion (error bars in histogram) of angular velocities of all the studied colloids (that completed a  $360^\circ$   
281 turn and rotated individually).

282

283 Using this procedure (fits of linear segments of orientation angle vs time), we calculated the angular  
284 velocity of the all the colloids in the presence of a rotating magnetic field. We used field intensities  
285 0.1 mT, 1 mT, 5 mT, 10 mT, 20 mT and rotational frequencies of 1 Hz and 5 Hz. A total of 400  
286 particles were analysed for the results presented in Fig. 4. Although over a hundred particles were  
287 analysed for each condition, only data for a relatively small number of particles was useful for  
288 quantitative analysis, since only particles able to perform at least a complete  $360^\circ$  turn were  
289 considered (including particles that performed backwards rotation movements and oscillations). The  
290 graphs indicate the fraction of particles that fulfil this criterion. It is important to note that a larger  
291 number of ellipsoidal particles were able to rotate individually (32.6% of particles agglomerated) in  
292 comparison to the majority of the commercial particles where the majority of particles (67.2%)  
293 agglomerated, making it harder to get a good sample number of rotating particles. The analysis of  
294 these uniform rotation segments in Fig. 4 shows that the performance of the ellipsoidal particles in  
295 terms of measured rotation frequency is similar to that of the commercial spherical particles,  
296 considering the measurement uncertainties. However, careful analysis of the data shows that  
297 commercial microparticles present a more irregular behaviour, especially at low magnetic fields  
298 (which are more interesting from an application point of view). Significantly, only 23 % of  
299 commercial particles analysed were able to individually complete at least a full  $360^\circ$  turn at 1 Hz,  
300 with this fraction being 26 % at 5 Hz on average over all magnetic field strengths. For instance, at the  
301 lowest magnetic field strength of 0.1mT, out of 10 commercial spherical particles assessed, only 4  
302 completed at least a full turn at 1Hz, and none at 5Hz. In comparison, our ellipsoidal particles  
303 displayed a clearly superior performance at all field strengths, with 77 % completing at least a full  
304 turn at 1 Hz, and 74 % at 5 Hz on average.

305



306

307 Figure 4. Angular velocities of colloids calculated with the procedure shown in Fig. 3 (fitting linear  
 308 segments of orientation angle vs time and averaging to obtain a mean particle rotation frequency) at  
 309 different intensities of the rotating magnetic field at (a) 1 Hz and (b) 5 Hz field rotation frequencies.  
 310 Ellipsoidal particles are shown in blue and commercial spherical particles are shown in red. Fractions at  
 311 the top of the bars show the numbers of particles that completed at least one full 360° cycle divided by  
 312 the total number of particles.

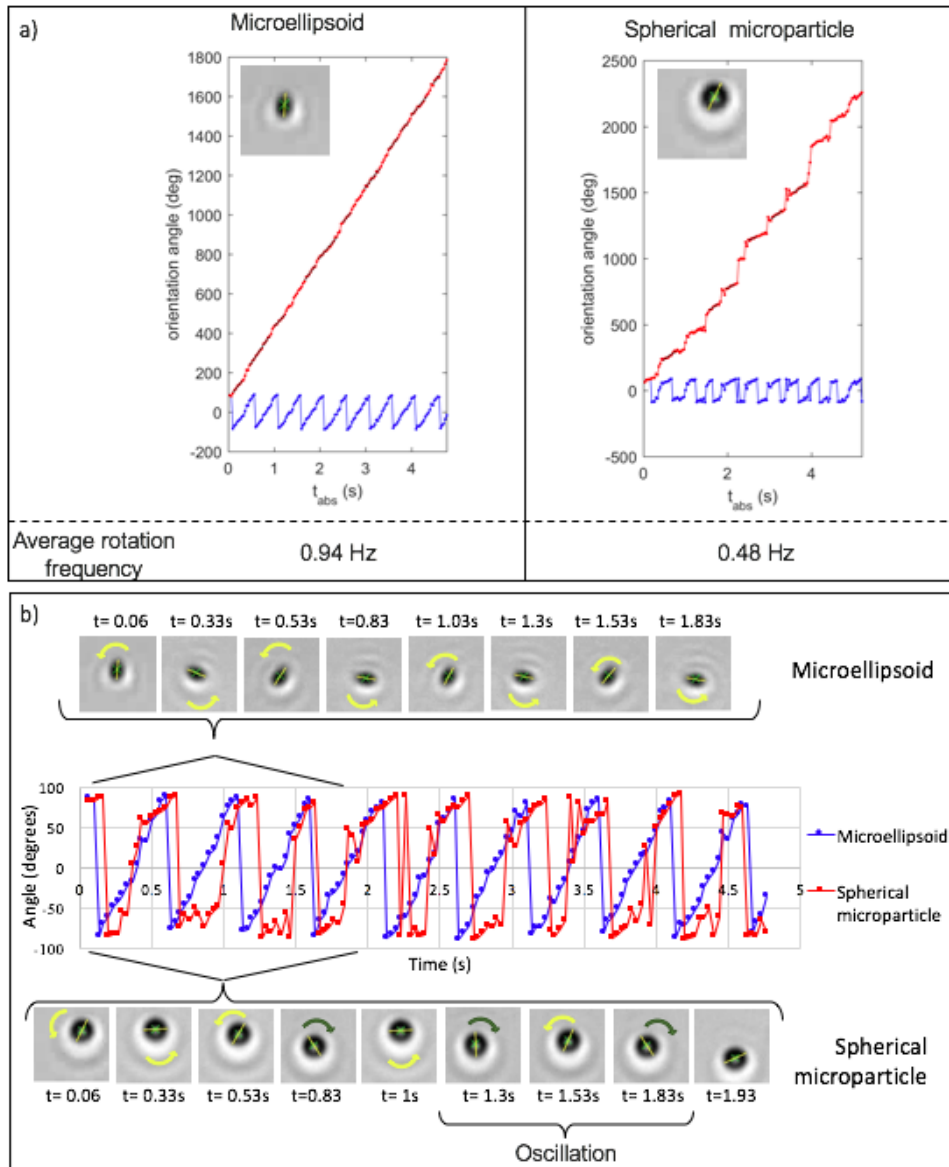
313

314 However, the previous analysis is not sufficient to evaluate the comparative performance of  
 315 the particles, especially at low intensities of the magnetic field (0.1 mT, 1 mT). At low field strengths,  
 316 the microellipsoids are able to smoothly follow the rotating magnetic field (see Video 1 in  
 317 supplementary information), whereas the commercial spherical microparticles do not follow the  
 318 field rotation smoothly and display oscillations in orientation, backwards rotation and jumps in  
 319 orientation (see Video 2 in supplement). Fig. 5 shows a comparison of two representative examples  
 320 of commercial microparticles and microellipsoids subject to a 1 mT, 1Hz magnetic field (Videos 1, 2  
 321 corresponding to these images are available in supplementary material).

322 Fig. 5 (a) shows the reasonably smooth rotation of the microellipsoid, whereas Fig. 5(b)  
 323 shows the angle versus time for the commercial spherical particle, which displays oscillations and  
 324 back and forth rotations. Although the spherical microparticle returns to its minimum orientation  
 325 angle (-90 degrees) as many times as the microellipsoid does, the microsphere does not actually  
 326 perform the same number of total turns as the microellipsoid. This is because the microsphere in  
 327 fact returns to the minimum angle by rotating backwards (green arrows) in some instances (see  
 328 video 2 in the supplement and Fig. 5(b)). Hence, the total number of turns per second is reduced to  
 329 0.48 Hz for the spherical microparticle, compared to 0.98 Hz for the microellipsoid (Fig. 5(a)).

330

1mT, 1Hz



331

332 Figure 5. Comparison of spherical (commercial) microparticles and microellipsoids as they are actuated by  
 333 a 1mT magnetic field rotating at 1Hz. (a) Representative examples of ellipsoidal (left) and spherical (right)  
 334 colloid orientation angle vs. time graphs. At the bottom of each graph, the corresponding average rotation  
 335 frequency (full rotation turns per second) is displayed for each case (see text). (b) Orientation  
 336 angle of ellipsoidal (blue) and spherical (red) colloids vs. time corresponding to the same data depicted in  
 337 (a). A sequence of images of the particle rotating at different times is included for the microellipsoid (top)  
 338 and the spherical microparticle (bottom). Arrows depict the rotation direction of the, displaying  
 339 oscillations and movement in the same (yellow arrows)/opposite (green arrows) direction to the applied  
 340 magnetic field for the commercial spherical microparticles (corresponding Videos 1 and 2 are given in  
 341 supplementary material). It is important to note that in the frames ( $t=0.83, 1s$  and  $1.83$  and  $1.93s$ ), the  
 342 microparticle turned to 0 degrees by rotating backwards. Some oscillation (back and forth change of the  
 343 angle) is also observed.

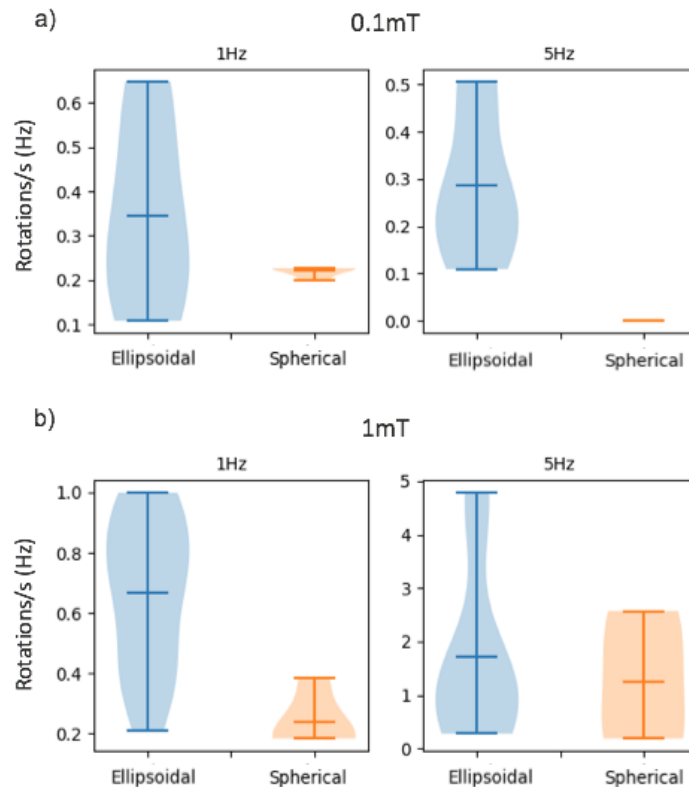
344

345            Since, at low magnetic fields, smooth rotation is not achieved for the spherical  
346 microparticles (Fig. 5 (b)), it is more useful, in order to compare their performance, to quantify the  
347 total number of full rotations per unit time observed from the videos. Fig. 6 shows violin plots of the  
348 number of full rotations per second for all the commercial microparticles and microellipsoids that  
349 completed at least one full turn, subject to a rotating field of (a) 0.1 mT and (b) 1 mT. These plots  
350 show the probability density of the data in order to visualise -in a more explicit way-, the amount of  
351 particles rotating a number of times per second and their distribution in each of the cases. Each side  
352 of the middle lines in each plot is a kernel density estimation and the distribution of the data. The  
353 wider regions of the violin plot show a higher probability of the component of the population to take  
354 a given value. Violin plots in figure 6 were smoothed by a kernel density estimator evaluated at 40  
355 points and were implemented using the Python.

356            For the 0.1mT, 1 Hz field, the microellipsoids rotated with a mean number of full rotations  
357 per second of  $(0.35 \pm 0.19)$  Hz, while this value was  $(0.22 \pm 0.01)$  Hz for the commercial  
358 microspheres. For the 0.1 mT, 5 Hz field, the microellipsoids' average number of full rotations per  
359 second was  $(0.29 \pm 0.15)$  Hz, while no commercial microparticle managed to perform a single full  
360 turn.

361            For the 1 mT, 1 Hz field, the average number of full rotations per second was  $(0.61 \pm 0.27)$  Hz  
362 for the microellipsoids and  $(0.26 \pm 0.13)$  Hz for the commercial particles. It is important to observe  
363 that the standard deviations for all field strengths and frequencies are larger for the microellipsoids  
364 than for the commercial particles. This is mainly due to a higher spread on rotation performance and  
365 a much larger number of assessed individual particles that complete at least one full turn for the  
366 microellipsoids compared to the commercial microparticles. This may be due to the different sizes of  
367 the microellipsoids and to variations in their magnetic (shape) anisotropy and/or inconsistent  
368 distribution of  $\text{Fe}_3\text{O}_4$  nanowires within the particles due to the lack of nanoscale control of the  
369 fabrication process.

370



371

372 Figure 6. Violin plots of the average number of full rotations per second for commercial spherical  
 373 microparticles (orange) and microellipsoids (blue) in the presence of (a) 0.1 mT and (b) 1 mT magnetic  
 374 fields rotating at 1 Hz (left) and 5 Hz (right).

375

376 Taking all the recorded particles into account (microellipsoids and spherical microparticles),  
 377 different behaviours were observed: from completely static particles -probably stuck to the bottom  
 378 of the container- to particles rotating only a few degrees back and forth, particles completing only  
 379 slightly less than a full 360 degree turn and particles moving backwards a few degrees and then  
 380 forwards in an oscillating manner (only spherical microparticles). Behaviour deviating from smooth  
 381 rotation in the direction of the field was mainly observed at the lowest intensities of the field and for  
 382 the commercial spherical microparticles. These are a result of the particles not reaching the  
 383 necessary energy to turn when trying to align with a rotating magnetic field. On the other hand, at  
 384 higher intensities of the field, spherical particles agglomerate more.

385 These results demonstrate that the synthesised ellipsoidal colloids outperformed the  
 386 spherical commercial microparticles at following the rotation of low magnetic fields. It is reasonable  
 387 to hypothesise that the relatively strong magnetic torque experienced by ellipsoids in the external  
 388 rotating magnetic fields (as compared to that exerted on the microspheres ) is mainly due to global  
 389 shape effects which create a deviation of the magnetization vector inside ellipsoids with respect to  
 390 the instantaneous direction of the applied field. This significant magnetic torque should allow a

391 smooth rotation of ellipsoids. Local magnetic susceptibility anisotropy effects cannot be completely  
392 ruled out as they can arise from complex effects due to the arrangement of the nanowires and their  
393 interactions within the microellipsoids [40]. But the smooth rotation (even at low fields) points  
394 towards a isotropic magnetic susceptibility within the ellipsoids, at least in the times and length  
395 scales probed here. The lower average effective rotation frequency measured for the commercial  
396 spherical microparticles and the appearance of oscillations and jumps in rotation are possibly due to  
397 their lower shape anisotropy (Fig. S.2 in the supplementary material). It is also possible that  
398 stochastic heterogeneities of the iron oxide distribution in the microspheres can lead to fluctuations  
399 of the magnetic torque and thus to fluctuations of the rotation speed of the particles. Furthermore,  
400 the thickness of the nanoparticle layer covering the spherical polystyrene core in the commercial  
401 particles might not be totally homogeneous for all the particles, producing some of the variability of  
402 their performance. It is also likely that the higher content of magnetic material for the commercial  
403 particles (approximately 20 times higher than in the microellipsoids) makes them heavier and more  
404 likely to adhere to the surface of the underlying substrate. The higher mass should also affect their  
405 moment of inertia.

406

#### 407 **4. Conclusions**

408 We report the synthesis of anisotropic, ellipsoidal microparticles following a novel, simple  
409 procedure based on the oil-in-water emulsion method. The microellipsoids are based on a lattice of  
410 biocompatible PCL with embedded  $\text{Fe}_3\text{O}_4$  nanowires; the ellipsoidal shape is achieved by using a  
411 magnetic field during synthesis. In order to evaluate the comparative advantage that ellipsoidal  
412 particles offer with respect to existing commercial spherical particles for magnetic control, we  
413 compared the rotational dynamics for both types of particles in magnetic fields with varying  
414 intensities (0.1, 1, 5, 10 and 20 mT) and rotational frequencies (1Hz and 5Hz).

415 Both commercial and ellipsoidal particles are able to follow smoothly magnetic fields at the  
416 higher field strengths (10 and 20 mT). However, at low field strengths (0.1 and 1 mT), commercial  
417 spherical particles present a lower effective average rotation frequency than the ellipsoidal particles,  
418 due to the occurrence of oscillations and jumps in rotation. A large proportion of commercial  
419 microparticles do not complete a single  $360^\circ$  turn. In total, only 23% of commercial particles  
420 analysed rotated for 1Hz fields and 26% for 5 Hz fields, whereas 77% of our ellipsoidal particles  
421 rotated at 1 Hz, and 74% did at 5 Hz. Furthermore, the number of individual commercial spherical  
422 microparticles able to rotate at higher field strengths (5, 10 and 20 mT) is very small (Fig. 4), owing to



423 aggregation of the particles with increasing field strengths. On the other hand, our microellipsoids  
424 were capable of full rotation individually at higher field strengths avoiding aggregation.

425 Our results show the superior rotation performance of the ellipsoidal particles in rotating  
426 magnetic fields in comparison to spherical commercial particles as expected from their intrinsic  
427 shape anisotropy, even though their magnetic material content is at least 20 times smaller than that  
428 of the commercial particles. The ellipsoidal shape makes the fabricated microellipsoids amenable to  
429 simple computational tracking and to theoretical calculations and modelling, which are key  
430 considerations for designing and fine-tuning future applications. The method presented here can be  
431 easily substituted for other top-down approaches such as 3D printing (size restricted to printer  
432 resolution), electrospraying [41], continuous-flow microfluidics [42, 43], soft lithography [44], etc.  
433 These methods could be fine-tuned by adapting them with other polymeric matrices and they  
434 present advantages over emulsification methods such as a better nanowire alignment, reduction of  
435 nanowire cluster formation -due to lack of rotational forces present during emulsification-,  
436 monodisperse size and ellipsoidal shape, control over the particle hardening process, uniform  
437 application of magnetic field, microparticle magnetic response optimisation, etc. However, these  
438 methods require infrastructure and expertise, which make them more unpractical for scaling-up as  
439 compared to the simple method presented in this paper.

440 Our simple fabrication and computational tracking method, along with a high (magnetic) shape  
441 anisotropy that allows for a better particle control using lower magnetic fields is than existing  
442 methods based on commercial microparticles, makes our ellipsoids good candidates for many of the  
443 applications mentioned in the introduction section, such as biophysical studies, magnetic tweezers,  
444 microfluidics, nucleic acid and protein manipulation, microrheology, torque-generating assays,  
445 magnetically directed drug delivery, etc.

446

#### 447 **Acknowledgements**

448 The author(s) would like to acknowledge networking support by the COST Action CA16122. ABB gratefully  
449 acknowledges support from a Mexican government CONACYT scholarship and support by a STSM Grant  
450 from COST Action CA16122.

451

#### 452 **Data availability**

453 All the experimental data will be deposited and made available through the Oxford Research Archive  
454 portal (<https://ora.ox.ac.uk/>).

455

456

## 457 **References**

458

459 [1] W.-l. Chiang, C.-j. Ke, Z.-x. Liao, S.-y. Chen, F.-r. Chen, C.-Y. Tsai, Y. Xia, H.-W. Sung, Pulsatile Drug  
460 Release from PLGA Hollow Microspheres by Controlling the Permeability of Their Walls with a  
461 Magnetic Field, *Small* 8(23) (2012) 3584-3588.

462 [2] O. Ergeneman, S. Gervasoni, B. Ozkale, P. Fatio, V.J. Cadarso, B.J. Nelson, Inkjet printed  
463 superparamagnetic polymer composite hemispheres with programmed magnetic anisotropy,  
464 *Nanoscale* 6(18) (2014).

465 [3] J. Thévenot, H. Oliveira, O. Sandre, S. Lecommandoux, Magnetic responsive polymer composite  
466 materials, *Chemical Society Reviews* 42 (2013) 7099-7116.

467 [4] R.M. Erb, J.J. Martin, R. Soheilian, C. Pan, J.R. Barber, Actuating Soft Matter with Magnetic  
468 Torque, *Advanced Functional Materials* 26 (2016) 3859-3880.

469 [5] A. Butykai, A. Orbán, V. Kocsis, D. Szaller, S. Bordács, E. Tátrai-Szekeres, L.F. Kiss, A. Bóta, B.G.  
470 Vértessy, T. Zelles, I. Kézsmárki, Malaria pigment crystals as magnetic micro-rotors: Key for high-  
471 sensitivity diagnosis, *Scientific Reports* 3 (2013) 1-10.

472 [6] O. Ergeneman, G. Chatzipirpiridis, J. Pokki, M. Marin-Suárez, G.A. Sotiriou, S. Medina-Rodriguez,  
473 J.F.F. Sanchez, A. Fernandez-Gutiérrez, S. Pane, B.J. Nelson, In vitro oxygen sensing using intraocular  
474 microrobots, *IEEE Transactions on Biomedical Engineering* 59(12 PART2) (2012) 3104-3109.

475 [7] S. Tottori, L. Zhang, F.M. Qiu, K.K. Krawczyk, A. Franco-Obregon, B.J. Nelson, Magnetic Helical  
476 Micromachines: Fabrication, Controlled Swimming, and Cargo Transport, *Adv Mater* 24(6) (2012)  
477 811-816.

478 [8] A. Rida, M.A.M. Gijs, Manipulation of Self-Assembled Structures of Magnetic Beads for  
479 Microfluidic Mixing and Assaying, *Analytical Chemistry* 76(21) (2004) 6239-6246.

480 [9] N. Pamme, Magnetism and microfluidics, *Lab on a chip* 1 (2006).

481 [10] V. Reenen, D. Jong, D. Toonder, M.W.J. Prins, Integrated lab-on-chip biosensing systems based  
482 on magnetic particle actuation : a comprehensive review *Lab on a Chip*, *Lab on a chip* 12 (2014).

483 [11] L. Chen, H. Zhang, L. Li, Y. Yang, X. Liu, B. Xu, Thermoresponsive hollow magnetic microspheres  
484 with hyperthermia and controlled release properties, *Journal of Applied Polymer Science* ·  
485 (September 2017) (2015).

486 [12] E.K. Paluch, C.M. Nelson, N. Biais, B. Fabry, J. Moeller, B.L. Pruitt, C. Wollnik, G. Kudryasheva, F.  
487 Rehfeldt, W. Federle, Mechanotransduction : use the force(s), *BioMed Central Biology* (2015) 1-14.

488 [13] W.J. Polacheck, C.S. Chen, Measuring cell-generated forces : a guide to the available tools,  
489 *Nature methods* 13(5) (2016) 415-423.

490 [14] M.M. Van Oene, L.E. Dickinson, B. Cross, F. Pedaci, J. Lipfert, N.H. Dekker, Applying torque to  
491 the *Escherichia coli* flagellar motor using magnetic tweezers, *Scientific Reports* 7 (2017) 1-11.

492 [15] M. Puig-de-morales, M. Grabulosa, J. Alcaraz, J. Mullol, G.N. Maksym, J.J. Fredberg, D. Navajas,  
493 M. Grabulosa, J. Al, J. Mullol, G.N. Maksym, J. Jeffrey, D. Navajas, Measurement of cell  
494 microrheology by magnetic twisting cytometry with frequency domain demodulation, *Journal of*  
495 *Applied Physiology* 91 (2001) 1152-1159.

496 [16] N. Wang, J.P. Butler, D.E. Ingber, Mechanotransduction Across the Cell Surface and Through the  
497 Cytoskeleton, *Science* 260(May) (1993) 1124-1128.

498 [17] C. Sun, H. Hassanisaber, R. Yu, S. Ma, S.S. Verbridge, C. Lu, Paramagnetic Structures within a  
499 Microfluidic Channel for Enhanced Immunomagnetic Isolation and Surface Patterning of Cells,  
500 Scientific reports (July) (2016) 1-9.

501 [18] H.-s. Lin, J.R. Carey, The Design and Applications of Nanoparticle Coated Microspheres in  
502 Immunoassays, Journal of Nanoscience and Nanotechnology 14(1) (2014) 363-377.

503 [19] A. Vila, V.C. Martins, A. Chícharo, C. Rodriguez-abreu, A.C. Fernandes, F.A. Cardoso, S. Cardoso,  
504 J. Rivas, P. Freitas, Customized Design of Magnetic Beads for Dynamic Magneto-resistive Cytometry,  
505 IEEE TRANSACTIONS ON MAGNETICS 50(11) (2014) 18-21.

506 [20] L. Clime, B.L. Drogoff, T. Veres, Dynamics of Superparamagnetic and Ferromagnetic Nano-  
507 Objects in Continuous-Flow Microfluidic Devices, IEEE TRANSACTIONS ON MAGNETICS 43(6) (2007)  
508 2929-2931.

509 [21] J. Faraudo, J.S. Andreu, C. Calero, J. Camacho, Predicting the Self-Assembly of  
510 Superparamagnetic Colloids under Magnetic Fields, Advanced Functional Materials 26 (2016) 3837-  
511 3858.

512 [22] S.-w. Cao, Y.-j. Zhu, M.-y. Ma, L. Li, L. Zhang, Hierarchically Nanostructured Magnetic Hollow  
513 Spheres of Fe<sub>3</sub>O<sub>4</sub> and  $\gamma$ -Fe<sub>2</sub>O<sub>3</sub> : Preparation and Potential Application in Drug Delivery, Journal  
514 of Physical Chemistry 112(6) (2008) 1851-1856.

515 [23] V.R. Dugyala, S.V. Daware, M.G. Basavaraj, Shape anisotropic colloids: synthesis, packing  
516 behavior, evaporation driven assembly, and their application in emulsion stabilization, Soft Matter  
517 9(29) (2013) 6711-6725.

518 [24] V.N. Paunov, O.J. Cayre, Supraparticles and "Janus" particles fabricated by replication of particle  
519 monolayers at liquid surfaces using a gel trapping technique, Adv Mater 16(9-10) (2004) 788-+.

520 [25] J.W. Kim, R.J. Larsen, D.A. Weitz, Synthesis of nonspherical colloidal particles with anisotropic  
521 properties, J Am Chem Soc 128(44) (2006) 14374-14377.

522 [26] R.G. Larson, The structure and rheology of complex fluids, Oxford University Press, New York ;  
523 Oxford, 1999.

524 [27] M.I. Mishchenko, J.W. Hovenier, L.D. Travis, Light scattering by nonspherical particles : theory,  
525 measurements, and applications, Academic Press, San Diego ; London, 2000.

526 [28] A.D. Dinsmore, M.F. Hsu, M.G. Nikolaidis, M. Marquez, A.R. Bausch, D.A. Weitz, Colloidosomes:  
527 Selectively permeable capsules composed of colloidal particles, Science 298(5595) (2002) 1006-  
528 1009.

529 [29] R.G. Alargova, D.S. Warhadpande, V.N. Paunov, O.D. Veleev, Foam superstabilization by polymer  
530 microrods, Langmuir 20(24) (2004) 10371-10374.

531 [30] S.C. Glotzer, M.J. Solomon, Anisotropy of building blocks and their assembly into complex  
532 structures, Nature Materials 6(8) (2007) 557-562.

533 [31] P.F. Noble, O.J. Cayre, R.G. Alargova, O.D. Veleev, V.N. Paunov, Fabrication of "hairy"  
534 colloidosomes with shells of polymeric microrods, J Am Chem Soc 126(26) (2004) 8092-8093.

535 [32] R.S.M. Rikken, R.J.M. Nolte, J.C. Maan, J.C.M.V. Hest, D.A. Wilson, P.C.M. Christianen,  
536 Manipulation of micro- and nanostructure motion with magnetic fields, Soft Matter 10 (2014) 1295-  
537 1308.

538 [33] J. Kim, S.E. Chung, S.-e. Choi, H. Lee, J. Kim, S. Kwon, Programming magnetic anisotropy in  
539 polymeric microactuators, Nature Materials 10(10) (2011) 747-752.

540 [34] V. Hessel, H. Lowe, F. Schonfeld, Micromixers - a review on passive and active mixing principles,  
541 Chem Eng Sci 60(8-9) (2005) 2479-2501.

542 [35] A. van Reenen, A.M. de Jong, J.M.J. den Toonder, M.W.J. Prins, Integrated lab-on-chip  
543 biosensing systems based on magnetic particle actuation - a comprehensive review, Lab on a Chip  
544 14(12) (2014) 1966-1986.

545 [36] M.M. van Oene, L.E. Dickinson, F. Pedaci, M. Kober, D. Dulin, J. Lipfert, N.H. Dekker, Biological  
546 magnetometry: torque on superparamagnetic beads in magnetic fields, Phys Rev Lett 114(21) (2015)  
547 218301.

- 548 [37] S. Lian, E. Wang, Z. Kang, Y. Bai, L. Gao, M. Jiang, C. Hu, L. Xu, Synthesis of magnetite nanorods  
549 and porous hematite nanorods, *Solid State Communications* 129 (2004) 485-490.
- 550 [38] M. Wang, H.J. Jin, D.L. Kaplan, G.C. Rutledge, Mechanical properties of electrospun silk fibers,  
551 *Macromolecules* 37(18) (2004) 6856-6864.
- 552 [39] J. Faraudo, J.S. Andreu, J. Camacho, Understanding diluted dispersions of superparamagnetic  
553 particles under strong magnetic fields: a review of concepts, theory and simulations (vol 9, pg 6654,  
554 2013), *Soft Matter* 9(48) (2013) 11709-11709.
- 555 [40] J.J. Wang, Y. Song, X.Q. Ma, L.Q. Chen, C.W. Nan, Static magnetic solution in magnetic  
556 composites with arbitrary susceptibility inhomogeneity and anisotropy (vol 117, 043907, 2015), *J*  
557 *Appl Phys* 119(6) (2016).
- 558 [41] H. Lee, S. An, S. Kim, B. Jeon, M. Kim, I.S. Kim, Readily Functionalizable and Stabilizable  
559 Polymeric Particles with Controlled Size and Morphology by Electro spray, *Scientific Reports* 8 (2018).
- 560 [42] L.A. Shaw, S. Chizari, M. Shusteff, H. Naghsh-Nilchi, D. Di Carlo, J.B. Hopkins, Scanning two-  
561 photon continuous flow lithography for synthesis of high-resolution 3D microparticles (vol 26, pg  
562 13543, 2018), *Opt Express* 26(11) (2018) 14718-14718.
- 563 [43] D. Dendukuri, D.C. Pregibon, J. Collins, T.A. Hatton, P.S. Doyle, Continuous-flow lithography for  
564 high-throughput microparticle synthesis, *Nature Materials* 5(5) (2006) 365-369.
- 565 [44] J.J. Guan, A. Chakrapani, D.J. Hansford, Polymer microparticles fabricated by soft lithography,  
566 *Chem Mater* 17(25) (2005) 6227-6229.

567

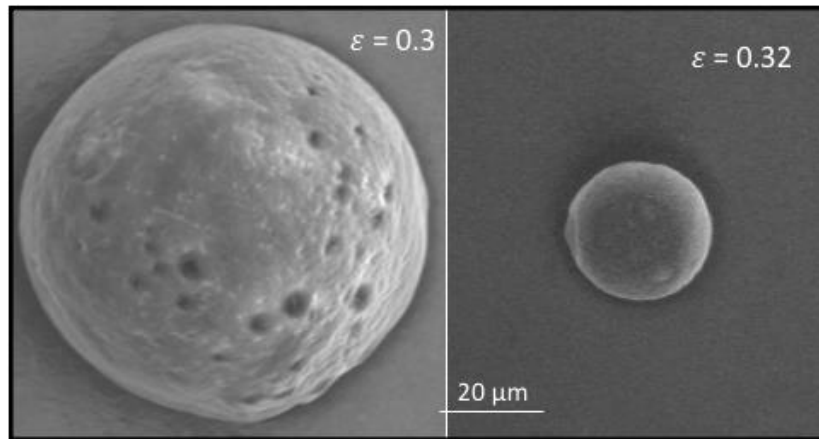
568

569

570 **Supplementary materials**

571 **A. Sphericity of colloids synthesised by oil-in-water emulsion with/without**  
572 **nanowires and with no applied magnetic field during hardening.**

573



574

575 **Figure A.1** SEM images of PCL colloids without nanowires and without magnetic field applied during the  
576 synthesis showing higher sphericity.

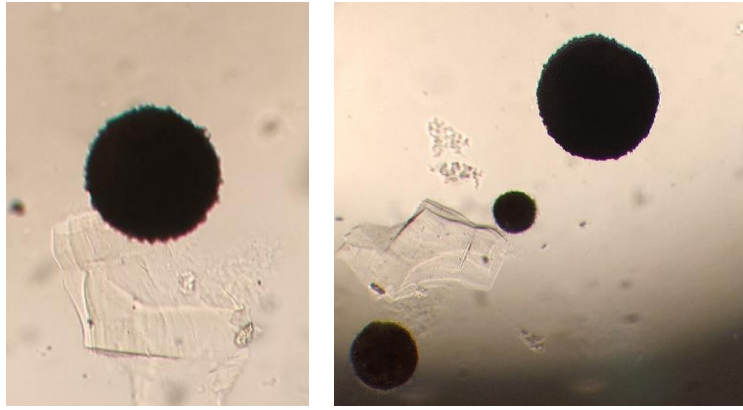
577

578 Figure A.1 shows colloids consisting of PCL synthesised by the same oil-in-water emulsion method as  
579 described in the microellipsoid synthesis section (oil phase consisting of Luperox 2.5% w/v and 0.5  
580 mM PCL dissolved in dichloromethane; water phase PVA 1.5% w/v; no nanowires embedded). These  
581 particles show higher sphericity in comparison to the ellipsoidal microparticles described in the main  
582 text (with 0.5% w/v magnetic  $\text{Fe}_3\text{O}_4$  nanowires embedded in the polymeric matrix and aligned in the  
583 presence of a 0.25T magnetic field during hardening).

584

585 Similarly, Figure A.2 shows an optical microscopy image of microparticles synthesised as  
586 described in the microellipsoid synthesis section without a magnetic field present during hardening  
587 as a control.

588



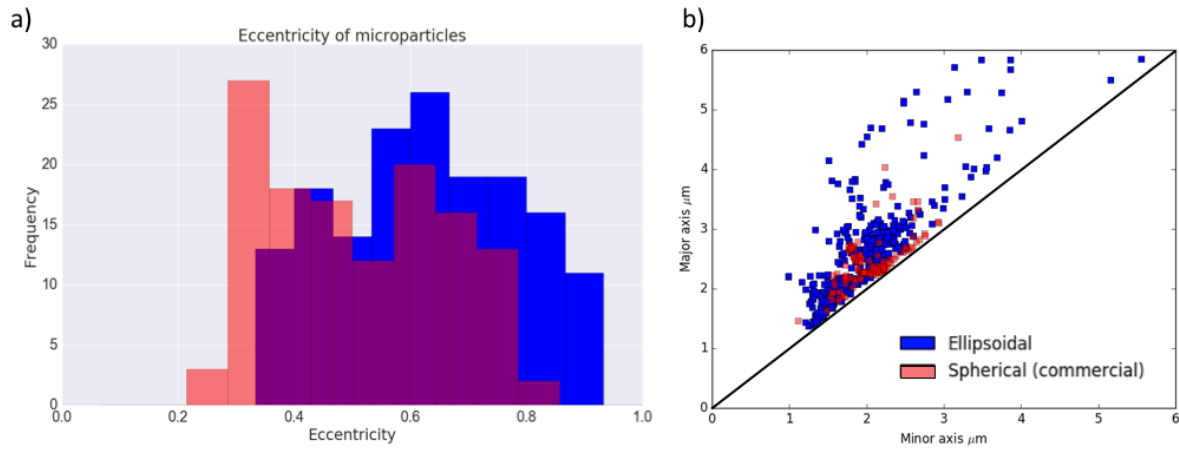
589

590

591 **Figure A.2. Optical microscopy image of microparticles of polycaprolactone and  $\text{Fe}_3\text{O}_4$  that were synthesized**  
592 **in the absence of a magnetic field, presenting a spherical shape, with  $\epsilon = 0.4 \pm 0.2$ .**

593 **B. Major and minor axis lengths of ellipsoidal and commercial spherical**  
594 **microparticles**

595



596

597

598 **Figure B.1** a) Histogram plot of the eccentricity of the commercial microparticles (red) against the ellipsoidal  
599 synthesised microparticles (blue). b) Minor vs. major axis of all of the analysed microparticles.

600

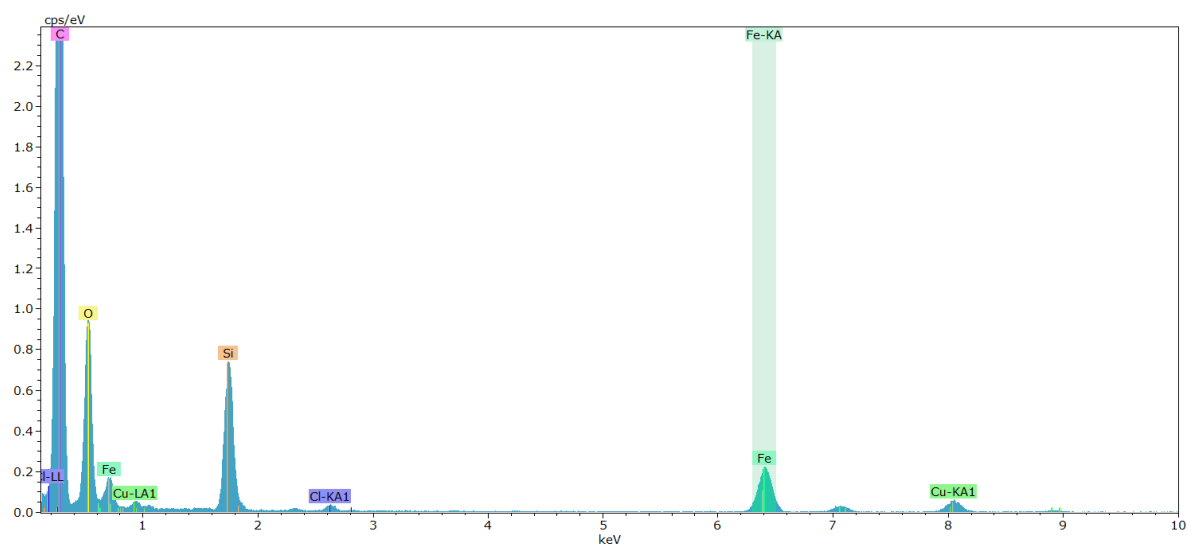
601 Figure B.1 a) shows a histogram of the eccentricity of both the ellipsoidal (blue) and the  
602 spherical (commercial) particles (red), calculated from the measured microparticle dimensions as  
603 explained in the image processing section. Eccentricity tends to zero with higher sphericity of the  
604 particle. It is apparent that the eccentricity of the commercial particles is smaller than that of the  
605 synthesised ones, with a mean value of the particle major axis  $2a = 2.48 \pm 0.55 \mu\text{m}$  and  $\epsilon = 0.40 \pm$   
606  $0.15$  for the commercial particles and  $2a = 2.68 \pm 1.10 \mu\text{m}$  and  $\epsilon = 0.60 \pm 0.14$  for the particles  
607 synthesised in this paper.

608 Figure B.1 b), shows a scatter plot of the major vs minor axis for all the analysed particles  
609 (synthesised particles in blue, commercial in red).

610

611

612 **C. TEM/ EDX Fe<sub>3</sub>O<sub>4</sub> nanowire structural composition analysis.**



613

614 **Figure C.1** EDX spectrum of Fe<sub>3</sub>O<sub>4</sub> nanowires synthesised as described in the materials and methods and  
615 shown in figure 2 (Results: Structural characterisation section).

616 The EDX analysis of the nanowires embedded in the PCL lattice shown in figure C.1 in the  
617 structural characterisation results section confirms the presence of Fe (0.72 and 6.40 keV), O (0.53  
618 keV) related to the Fe<sub>3</sub>O<sub>4</sub> nanowires and C (0.27 keV) related to the polymeric PCL lattice.

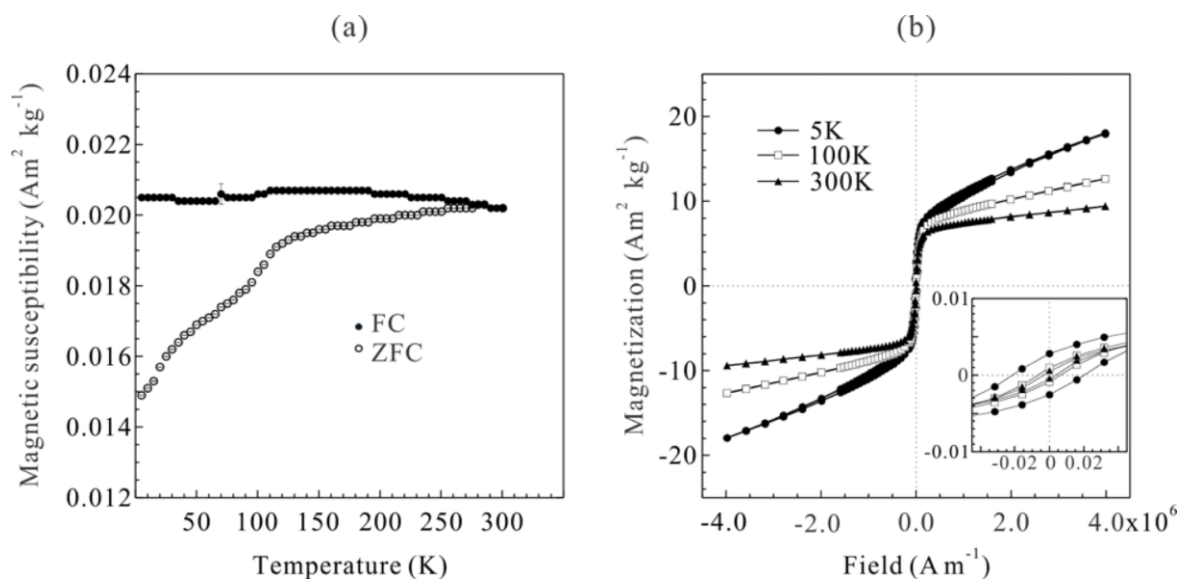
619

620



621  
622

## D. Nanowire magnetic characterisation: superconducting quantum interference device (SQUID) Measurements



623  
624  
625  
626  
627

Figure D1. (a) Zero field cooled (ZFC) and field-cooled (FC) magnetic susceptibility curves for a sample of  $\text{Fe}_3\text{O}_4$  nanowires measured using a field of  $796 \text{ A m}^{-1}$  in the range  $5 \leq T \text{ (K)} \leq 300$ . (b) The magnetization isotherms at  $T = 5, 100, 300 \text{ K}$  and field range  $-3.98 \leq H \text{ (} \times 10^6 \text{ A m}^{-1} \text{)} \leq 3.98$ . Inset: enlargement of the coercive zone.

628 In figure D1 a) we can see a feature at  $T \approx 120 \text{ K}$  both in the zero field cooled (ZFC) and field  
629 cooled (FC) curves that corresponds well to the Verwey transition for  $\text{Fe}_3\text{O}_4$  samples in the  
630 nanoscale [3] although no temperature in the measurement window seems to correspond to the  
631 blocking temperature (TB). The ZFC and FC curves diverge throughout the whole range of  
632 temperatures measured suggesting that the TB is greater than 300 K.

633 A value of TB greater than 300 K is in agreement with the coercivity observed in the M/H  
634 isotherms shown in Figure D1 b). As shown in the inset, the coercive field  $H_C$  decreases upon  
635 heating from 5 to 100 K, from  $21.52 \times 10^3$  to  $6.68 \times 10^3 \text{ A m}^{-1}$  (where  $1/4\pi \text{ A m}^{-1} = 1 \times 10^{-3} \text{ Oe}$ ).  
636 However, at 300 K, an  $H_C$  of  $3.35 \times 10^3 \text{ A m}^{-1}$  is still observed. An  $H_C$  of approximately  $0 \text{ A m}^{-1}$   
637 would be expected from a superparamagnetic behaviour. Nevertheless, the observed value  $H_C =$   
638  $3.35 \times 10^3$  is in good agreement with previously reported values of  $H_C$  for  $\text{Fe}_3\text{O}_4$  nanowires and  
639 nanoparticles at 300 K. [3],[2].

640 The saturation magnetization ( $M_S$ ) was not reached during the collection of the M/H isotherms  
641 even at an applied field of  $3.98 \times 10^6 \text{ A m}^{-1}$  (5 T). The maximum magnetizations registered at the  
642 maximum applied field are 18.05, 12.66 and  $9.41 \text{ Am}^2 \text{ Kg}^{-1}$  ( $1 \text{ Am}^2 \text{ Kg}^{-1} = 1 \text{ emu g}^{-1}$ ) for the  
643 isotherms at 5, 100 and 300 K respectively. Remanent saturation magnetization values of 10.22,  
644 7.87 and  $6.90 \text{ Am}^2 \text{ Kg}^{-1}$  can be extracted from extrapolation of M versus  $1/H$  plots. These rather  
645 small values for the magnetization can be explained from the random orientation of the  $\text{Fe}_3\text{O}_4$   
646 nanowires during our measurements [4]. The magnetic domains in the  $\text{Fe}_3\text{O}_4$  nanowires sample

647 can be found oriented parallel, perpendicular and even antiparallel with respect to the applied  
648 magnetic field, thus hindering the observed overall magnetic moment [4].

649 The shape of the ZFC and FC curves is also consistent with previous reports in the literature for  
650  $\text{Fe}_3\text{O}_4$  nanowire arrays of diameters in the range of 100 to 200 nm [4]. The breadth of both curves  
651 can be explained from a distribution of sizes of the nanowires, which leads to a distribution of  
652 values for the magnetic susceptibility as the temperature approaches TB.

653 Interactions between nanowires can shift HC to smaller or higher values depending on local  
654 ordering and orientation of the easy axis [1].

655

## 656 **References**

657

658 [1] Castellanos-Rubio, I.; Insausti, M.; Garaio, E.; Gil de Muro, I.; Plazaola, F.; Rojo, T.; Lezama, L.  
659 *Nanoscale* 2014, 12, 7542.

660 [2] Han, R.; Li, W.; Pan, W.; Zhu, M.; Zhou, D.; Li, F. *Sci. Rep.* 2015, 4 , 7493.

661 [3] Yang, J. B.; Xu, H.; You, S. X.; Zhou, X. D.; Wang, C. S.; Yelon, W. B.; James, W. J. *J. Appl. Phys.*  
662 2006, 99 , 08Q507.

663 [4] Zhang, L.; Zhang, Y. *J. Magn. Magn. Mater.* 2009, 321, L15.

664

665

666